ANCF Analysis of Multibody Pantograph/ Catenary Systems

BY

SHUBHANKAR KULKARNI
B.E. Mechanical Engineering
University of Pune, 2012

THESIS

Submitted as partial fulfillment of the requirements
for the degree of Master of Science in Mechanical Engineering
in the Graduate College of the
University of Illinois at Chicago, 2016

Chicago, Illinois

Defense Committee:

Ahmed A. Shabana, Chair and Advisor, Mechanical Engineering
Eduard Karpov, Civil Engineering
Marina Gantoi, Sharma and Associates, Inc.

ACKNOWLEDGEMENTS

I would like to thank my advisor, Dr. Ahmed A. Shabana for giving me an opportunity and his continued support and guidance throughout this work. His constant motivation inspired me to complete the research. I am thankful to Prof. Eduard Karpov and Dr. Marina Gantoi for agreeing to be a part of my thesis committee.

I would also like to thank all my laboratory mates of Dynamic Simulation Laboratory, especially Dr. Carmine M. Pappalardo, who helped me with any obstacles I faced during my research.

I am grateful to my parents for their continuous support and encouragement. Lastly I would like extend my gratitude to all my friends who were very supportive and made me feel at home in Chicago.

TABLE OF CONTENTS

LIST OF TABLES

LIST OF FIGURES

LIST OF FIGURES (Continued)

SUMMARY

The high speed trains today most commonly use pantograph-catenary systems for power delivery. The dynamics of the pantograph-catenary system plays a crucial role in the current collection quality and, therefore, thorough computational modeling is required to correctly predict the dynamical behavior of this complex system. In this investigation, a multibody pantograph model is used along with the absolute nodal coordinate formulation (ANCF) based catenary model to simulate the pantograph-catenary system in the multibody dynamics environment. To this end, the ANCF cable elements are used to model the contact wire and the messenger wire. Furthermore, a new contact formulation based on the penalty force approach is presented to study the interaction between the pan-head and the contact wire. This new formulation is derived from the sliding joint model proposed in the literature. The contact model developed in this work can be employed with the fully parameterized as well as the gradient deficient ANCF based finite elements. The loss of contact between the pan-head and the overhead contact line can be modeled with this new contact formulation. On the other hand, the pantograph model is mounted on a detailed rail- vehicle model allowing to evaluate more realistic situations. The contact between the rail vehicle wheels and the track is modeled using the elastic contact approach. One of the other major factors affecting the contact force is the external aerodynamic forces acting on the pantograph components and the catenary system as well. Two scenarios are considered where crosswind loading is applied on just the pantograph components, and aerodynamic forces applied on the pantograph and also the flexible catenary. In this study, the time varying nonlinear aerodynamic forces are modeled, thereby capturing the influence of the aerodynamic forces on the dynamical behavior of the pantograph-catenary system.

SUMMARY (Continued)

For the configuration considered in this work, the effect of the crosswind is that it assists the uplift force exerted on the pantograph mechanism increasing the mean contact force value. Numerical results are compared for the cases for with and without the wind forces.

CHAPTER 1

INTRODUCTION

Pantographs are mechanical systems mounted on the top of the rail vehicles for the purpose of collecting current from an overhead contact line carrying power. An uplifting mechanism keeps the pantograph current collectors or the pan-head in the contact with the contact wire. The pantograph-catenary systems are the most feasible way to power high speed trains which travel at the speed of more than 300 km/h (Bruni et al., 2012; Bruni and Facchinetti, 2012; Facchinetti et al., 2013).

The dynamics of the pantograph-catenary system plays a crucial role in maintaining a consistent current collection quality in the high-speed trains. The vibrations in the car body or adverse weather conditions can affect the interaction between the pantograph pan-head and the overhead contact line, which may result into severe problems like arcing or damaged components. Unfavorable operating conditions or inefficient design can result into high wear rates and hence a shorter fatigue life of the pan-heads and the catenary system, increasing the maintenance costs significantly. The wear rates are governed by several parameters such as the sliding speed, current intensity, contact force and also the nature of the materials in contact (Bucca and Collina, 2009). Hence, analyzing the contact forces between the pantograph and the catenary is given a prime importance to ensure smooth power delivery and optimized wear of the components.

The field of multi-body dynamics has matured over the last couple of decades to efficiently model the dynamics of the rigid and the flexible bodies as well. This framework has proved to be very useful in wide range of applications including the automotive and the aerospace industries, machinery industry, railroad vehicle applications and many more. A multi-body system consists of rigid and flexible bodies connected with each other by means of joints or constraints. A large amount of research effort has been put into developing new formulations to accurately capture deformations of flexible bodies in the dynamic analysis. In the case of rigid multibody systems, the principal methods employed to analytically describe the motion of a mechanical system are the relative or recursive coordinate formulation, the reference point coordinate formulation and the natural coordinate formulation (Bae and Haug, 1987A; Bae and Haug, 1987B; Garcia de Jalon, 2007; Pappalardo, 2015). On the other hand, formulations like floating frame of reference are used to capture the small deformations of the bodies having large displacements. The coordinate formulations like the absolute nodal coordinate formulation (ANCF) have proved to be very effective in cases where large rotations and large deformations are employed (Shabana, 1998; Shabana and Yakoub, 2000; Yakoub and Shabana, 1998).

Multibody dynamics simulations can provide an effective environment to study the pantograph-catenary interaction and to estimate the contact forces (Gerstmayr and Shabana, 2006; Pappalardo et al., 2015; Seo et al., 2005; Seo et al., 2006). The effect of aerodynamic forces can be taken into account simultaneously as well, which is important in determining the required uplift force for the pantograph mechanism and also in defining the control strategy for the contact force. This is needed as the drag and the lift component of the aerodynamic forces can impart instability into the system by means of fluid- structure interaction resulting into unexpected behavior of the system or it may even damage the system severely. Therefore, to have a more realistic model to predict correct behavior of the pantograph system it is necessary to account for the aerodynamic forces in the model (Pombo et al., 2009; Stickland and Scanlon, 2001).

In the previous studies of the pantograph-catenary interaction, several different methods have been applied to model the system and compute the contact forces. The first method uses partial differential equations to mathematically represent the catenary as a continuous string or beam (Arnold and Simeon, 2000). Although these models are easy to solve, they have limitations in capturing the wave propagation and high frequencies involved in the pantograph-catenary interaction. A higher number of discretization points and smaller time steps are required to solve catenary equations for accurate numerical results (Poetsch et al., 1997). The second method uses linear finite elements to model the catenary (Collina and Bruni, 2010; Massat et al., 2006; Pombo et al., 2009; Pombo et al., 2012). In these models, the moving contact force is applied as an external force on the catenary (Ambrosio et al., 2009; Poetsch et al., 1997). In this case, a co-simulation technique is used between a finite element analysis code where the catenary is modeled and a multibody dynamics code where the pantograph is modeled. The third method uses ANCF finite elements to model the catenary to capture the geometric nonlinearities more accurately (Lee and Park, 2012; Pappalardo et al., 2015; Seo et al., 2005; Seo et al., 2007). The need for co-simulation is eliminated in this method as the ANCF catenary and the rigid pantograph are modeled in one single multi-body dynamics framework. A benchmark study of the pantograph-catenary system simulation presented by Bruni et al. (2015) involves multiple cases where the pantograph is modeled in a multibody dynamics environment and the catenary being modeled as Euler- Bernoulli linear beam elements. A catenary model created with ANCF beam elements is also benchmarked in the study.

Through a wide range of applications, ANCF has come up as an effective formulation to capture the large rotations and large deformations in the multibody dynamics framework. The ANCF uses nodal absolute positions and nodal position vector gradients as generalized coordinates for defining the kinematics of a finite element. This particular choice for the generalized coordinates leads to the separation of variable property in the kinematical description of the element position field and, therefore, the ANCF finite elements have a constant mass matrix and zero Coriolis and centrifugal inertia forces. Different elements have been developed using this formulation from which the three- dimensional beam element and the cable element can be of particular interest to this investigation (Shabana, 2010). The ANCF beam element is consistent with the geometrically exact formulation of the general theory of continuum mechanics and can capture the deformation of the cross-section. The ANCF cable element, on the other hand, leads to a more efficient implementation because it is a gradient deficient element and, therefore, the computation of the element generalized elastic forces is computationally less intensive. The only limitation of the cable element being that it cannot describe rotation about its own axis. This limitation not being a big hurdle in the catenary system modeling, it can be effectively used with the right contact model for this particular investigation.

There are mainly two methods used to model the contact force, the first being a constraint based approach and the second being the elastic contact approach (Pappalardo et al., 2015). The constraint based approach or the sliding joint formulations impose constraints at the contact point on the pantograph pan-head and the catenary. These constraints are formulated in terms of algebraic equations that are satisfied at the position, velocity and acceleration levels. The contact force is applied on both the bodies as a result of imposed constraints. The constraint based approach can avoid high frequencies involved as the contact force is applied as a constraint force. However, these constraints do not allow to model loss of contact phenomenon. This phenomenon can occur due to large vibrations in the rail vehicle body or extreme weather conditions (Seo et al., 2005). The elastic contact or the penalty approach uses a virtual springdamper system producing a unilateral force that allows for the separation of the two-body contact. This force is applied as an external force on both, the pantograph and the flexible contact wire. Even though penalty contact formulation is easier to implement, determining suitable penalty coefficients for capturing the wanted dynamical behavior can be challenging depending on the physics of the problem. To this end, a Hertzian type of contact force model proposed by Lankarani and Nikravesh (1994) is used in the earlier investigations.

The weather conditions have a major impact on the pantograph-catenary interaction (Bacciolone et al., 2006; Carnevale et al., 2015; Pombo et al., 2009). The main factors are the temperature and the wind. High temperature can modify the static position and the tension in the catenary. This condition does not have a significant impact on straight tracks. Cold weather conditions may result into formation of ice on the wires resulting into some deformation. Wind forces disturb the catenary system position and also influence the pantograph components directly. The drag and the lift forces can cause the mean contact force value to change. When pantographs with multiple collectors are considered, the aerodynamic forces can introduce an unbalance between the front and the rear collectors causing uneven wear. Very high wind forces can impact the catenary system significantly causing it to oscillate with large amplitudes. The worn out overhead contact line shape may generate asymmetric drag and lift forces resulting into the galloping motion of the catenary system (Stickland and Scanlon, 2001; Stickland et al., 2003). Hence, assessing the effect of aerodynamic forces on the pantograph and the catenary becomes important while designing the current collection systems so as to maintain a continuous and consistent contact between the pan-head and the contact wire with an optimum uplift force so as to minimize the wear of the components. To avoid this contact force unbalance, usually spoilers are placed on the collectors or the pan-head geometry is optimized such that the effect of aerodynamic pitching moment is minimized. There are two main approaches used for simulating the effect of the aerodynamic forces on the pantograph-catenary systems. In the first approach, computational fluid dynamics (CFD) is used to compute the aerodynamic forces on individual components of the pantograph and ultimately assess the contribution of the wind forces to the total uplift force on the pantograph (Bacciolone et al., 2007; Carnevale et al., 2015). In the second approach, the drag and the lift coefficients for the individual pantograph components are obtained from experimental studies and the aerodynamic forces are computed using the equation $\mathbf{F} = \left(\frac{1}{2} \rho (CA) \left| \mathbf{v}_{rel} \right|^2 \right) \hat{\mathbf{v}}$ (Pombo et al., 2009), where $\mathbf{F}$ is the drag or the lift force, ρ is the density of the fluid, *(CA)* is the drag or the lift pressure coefficient and $\mathbf{v}_{rel}$ is the relative velocity between the wind and the pantograph component, and $\hat{\mathbf{v}}$ is the unit vector in the direction of the drag or the lift force.

In the presented study, the absolute nodal coordinate formulation (ANCF) based thin Euler-Bernoulli beam or the cable elements are used to model the contact wire and the messenger wire (Bruni et al., 2014; Gerstmayr and Shabana, 2005; Pappalardo et al., 2015; Seo et al., 2005; Seo et al., 2007). The ANCF method is used because it can model the large deformations and geometric nonlinearities in the catenary effectively. The pantograph is built as a multibody mechanism which captures the nonlinear dynamics of the system properly. The pantograph mechanism is constructed on top of a detailed rail vehicle multibody model. A new contact formulation based on the elastic contact approach is presented in this study to model the pantograph-catenary interaction, which can be used with gradient deficient as well as the fully parameterized ANCF finite elements as only a single gradient vector is needed in the contact model. In the formulation of the contact forces between the pantograph pan-head and the contact wire, the arc length of the catenary is used as a non-generalized coordinate to exactly determine the location of the contact point on the catenary. One of the contact formulation constraint equations is solved for the non-generalized arc length coordinate using Newton- Raphson iterative method. Once this parameter is determined, the other contact constraint equations are imposed using a penalty force approach which ultimately compute the contact force. The contact force is applied as an external force on the pan-head and the flexible overhead contact line at the point of contact. The presented contact method can model the loss of contact scenario as well, which cannot be modeled using the sliding joint formulations presented in earlier investigations which used ANCF to model the catenary. The effect of the aerodynamic forces on the individual pantograph components and the catenary is also considered in the model. The effect of the crosswind on the dynamics of the pantograph-catenary interaction is analyzed and compared with the case where the wind effect is not considered.

The thesis is organized as follows. In Chapter 2, the rigid multibody models of the rail vehicle and the pantograph are described. Chapter 3 discusses the flexible catenary model. In Chapter 4, the new formulation for the contact force and the new method to compute aerodynamic forces is discussed in detail. The formulation used for the wheel- rail contact is also included. Chapter 5 is dedicated for the results and discussions. Conclusions from this investigation are conferred in Chapter 6.

CHAPTER 2

RAIL VEHICLE AND PANTOGRAPH MECHANISM MODEL

This chapter describes the rigid multi-body models of the rail vehicle and the Faiveley Transport CX pantograph used. These models can be used for general purpose rail-road dynamics studies as well.

2.1 Rail Vehicle Multi-body System Model

A detailed general purpose rigid-body rail vehicle model is used in this investigation, which is shown in the Fig. 1. The model has one car body with two bogies. The bogie consists of six bodies, two wheelsets, two equalizers, a bolster and a frame. The equalizers are connected to the frame, and the frame to the bolster using the bushing elements. Wheelsets are connected to the equalizers using the bearings. The bolsters are attached to the car body using revolute joints. In all, the model consists of 14 rigid bodies, 48 bushing elements, 8 bearings and 2 revolute joints. The rigid-body model parameters are defined in Table 1. A three-dimensional wheel rail contact has been defined which will be described in Chapter 3.

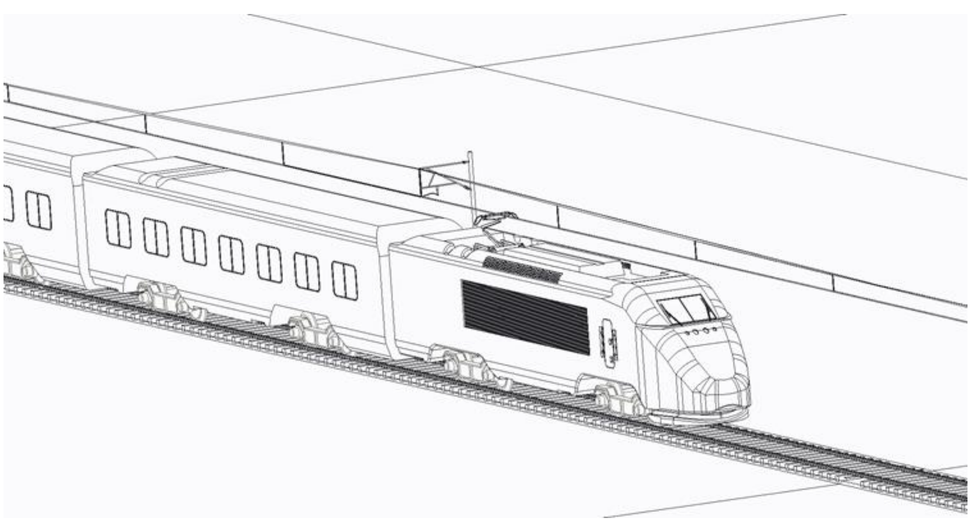

Figure 1. Rail vehicle system schematic (Pappalardo et al., 2015)

Table 1. Rail vehicle model data

Body	**Mass** (kg)	**Inertia** (kg·m^2)			**Initial Position** (m) (x^i_0, y^i_0, z^i_0)
		I_{xxi}	I_{yyi}	I_{zzi}	
Wheelsets	2091	1098	191	1098	0, 0, 0.4570488
					2.5908, 0, 0.4570488
					12.573, 0, 0.4570488
					15.1638, 0, 0.4570488
Equalizers	469	6.46	255	252	1.2954, 1.0287, 0.3049427
					1.2954, -1.0287, 0.3049427
					13.8684, 1.0287, 0.3049427
					13.8684, -1.0287, 0.3049427
Frame	3214	1030	1054	2003	1.2954, 0, 0.5081427
					13.8684, 0, 0.5081427
Bolster	1107	498	20.4	458	1.2954, 0, 0.7088
					13.8684, 0, 0.7088
Car Body	24170	30000	687231	687231	1.8289, 0, 1.8289

2.2 *Pantograph Multi-body System Model*

A multibody system model of a Faiveley Transport CX pantograph is analyzed in this investigation (Pappalardo et al., 2015; Pombo et al., 2009). The pantograph consists of six rigid-body parts interconnected with each other using revolute and spherical joints. The kinematic constraint data is provided in Table 3. The inertia properties as well as the global initial position and the orientation parameters are specified in Table 2. The orientation parameters are given in terms of Euler angles. The local coordinate system for each component is located at the center of mass and is oriented such that the orientation of the axes is defined to be aligned with the principal inertia directions. Figure 2 shows a schematic of the pantograph-catenary system as a whole.

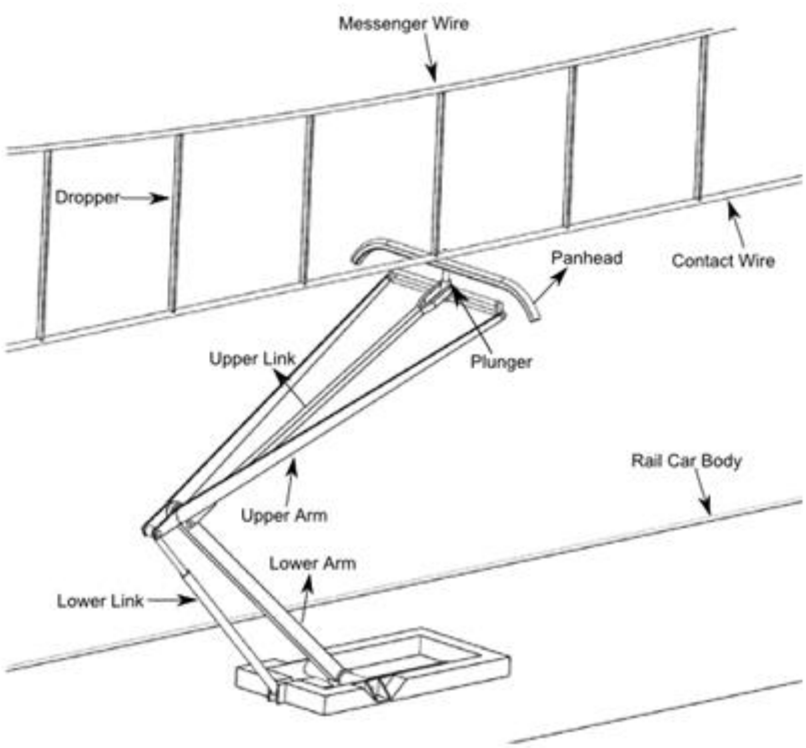

Figure 2. Pantograph-catenary model schematic (Pappalardo et al., 2015)

Table 2. Pantograph model data

Body	**Mass** (kg)	**Initial Position** (m) (x^i_0, y^i_0, z^i_0)	**Initial Orientation** (φ, θ, ψ)	**Inertia** (kg·m^2) $(I_{xxi}, I_{yyi}, I_{zzi})$
Lower arm	32.18	11.26924156, 0, 3.84511275	$\pi/2$, 0.5528807212, $-\pi/2$	0.31, 10.43, 10.65
Upper arm	15.60	11.45796454, 0, 4.52440451	$-\pi/2$, 0.2896816713, $\pi/2$	0.15, 7.76, 7.86
Lower Link	3.10	10.96436876, 0, 3.81940451	$\pi/2$, 0.6234559506, $-\pi/2$	0.05, 0.46, 0.46
Upper link	1.15	11.58587608, 0, 4.49940451	$-\pi/2$, 0.3028168645, $\pi/2$	0.05, 0.48, 0.48
Plunger	1.51	12.5, 0, 4.835	0, 0, 0	0.07, 0.05, 0.07
Pan-head	9.50	12.5, 0, 4.945	0, 0, 0	1.59, 0.21, 1.78

Table 3. Pantograph model joints data

First Body	Second Body	Joint Constraint
Car Body	Lower Arm	Revolute
Lower Arm	Upper Arm	Revolute
Upper Arm	Plunger	Revolute
Car Body	Lower Link	Spherical
Upper Arm	Lower Link	Spherical
Plunger	Upper Link	Spherical
Lower Arm	Upper Link	Spherical

CHAPTER 3

FLEXIBLE MULTIBODY MODEL OF THE CATENARY WIRES

The general catenary system consists of two wires- a contact wire and a messenger wire. The contact wire is in contact with the pantograph pan-head. The messenger wire holds the contact wire from sagging due to its self-weight. The contact wire is connected to messenger wire using droppers. Supporting poles are placed at certain distances so as to support the messenger wire and the contact wire. The contact wire is suspended with the help of a registration arm, which has low inertia. The general construction of the catenary system is shown in the Fig. 3.

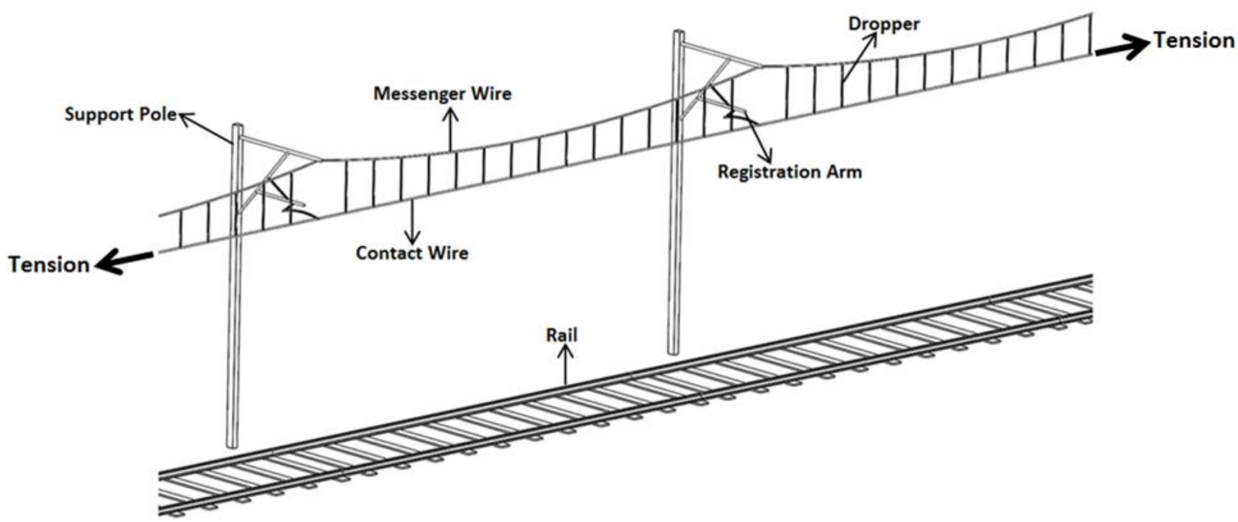

Figure 3. The Catenary System (Pappalardo et al., 2015)

The contact wire has a cross-section area of about 65-150 mm^2 and a span of about 50-65 m. The contact wire is usually made of high electrical conductivity materials such as steel alloys or copper alloys. The catenary system carries around 1000 V to 25,000 V of power depending on the type of trains it is used for. The droppers are tensile elements and virtually have zero stiffness in compression. At high speeds, the wave propagation speed in the contact wire becomes an important parameter of consideration so as to maintain a consistent contact between the pantograph and the wire. The wave propagation speed is directly depends on the beam bending stiffness, length of the beam and the tension in the beam (Ambrosio et al., 2012). At high speeds, the tension is the key parameter that affects the wave propagation speed, the effect of bending stiffness becomes negligible. Hence, tensioning of the catenary system plays a crucial role in the current collection quality and the speed limit of the train. The tension values typically range between 14- 40 kN depending on the operating speed of the train. In this investigation, the contact wire and the messenger wire are modeled using the absolute nodal coordinate formulation.

3.1 ANCF Finite Elements

The catenary goes under deformation in the region where it is in contact with the pantograph. The structure of the catenary is geometrically nonlinear. As mentioned earlier, various methods have been used to model the catenary system so as to capture its behavior such as modeling the contact wire using PDEs, linear Euler- Bernoulli beam elements, the Fourier sine expansion method, and ANCF finite elements- fully parameterized beam elements as well as the cable elements. The ANCF beam and cable elements can capture the nonlinear geometry of the catenary and the wave propagation phenomenon in the contact wire. The contact formulations can be systematically implemented with the ANCF beam elements as shown in the previous studies (Pappalardo et al., 2015; Seo et al., 2005; Seo et al., 2007). The ANCF cable element is used in this study, which uses the global position and only a single position vector gradient to define the element displacement field (Gerstmayr and Shabana, 2005). The global position of an arbitrary point on a flexible body is defined as $\mathbf{r}(\mathbf{x},t)=\mathbf{S}(\mathbf{x})\mathbf{e}(t)$, where $\mathbf{x}=[x \quad y \quad z]^T$ is the vector of the element spatial coordinates, $\mathbf{S}=\mathbf{S}(\mathbf{x})$ is the matrix of space dependent element shape functions, and $\mathbf{e} = \mathbf{e}(t)$ is the vector of the time dependent element nodal positions and slopes. For an element j of the cable element, the vector of nodal coordinates $\mathbf{e}^j = \mathbf{e}^j(t)$ is defined as:

$$\mathbf{e}^{jk} = \left[\left(\mathbf{r}^{jk}\right)^T \quad \left(\mathbf{r}_x^{jk}\right)^T \right]^T \quad , \quad k = 1, 2 \tag{1}$$

where k refers to the element node number, $\mathbf{e}^j = \left[\left(\mathbf{e}^{j1}\right)^T \quad \left(\mathbf{e}^{j2}\right)^T \right]^T$ is the vector of the element coordinates, $\mathbf{r}^k = \mathbf{r}^k(\mathbf{x}, t)$ is the global position vector of the node k, and $\mathbf{r}_x^k = \mathbf{r}_x^k(\mathbf{x}, t)$ represents the element gradient at the respective node k. For the coordinates chosen for the cable element, the rotation of the beam about its own axis cannot be described and therefore is not suitable for pure torsional effects. In the application of the cable element to the catenary modelling, the torsional effects are negligible and hence cable element can be effectively used to capture the bending effects. The ANCF cable element has half of the degrees of freedom of the fully parameterized ANCF 3D beam element and no stiff terms related to shear deformation. The shape functions of the element are given by:

$$\left.\begin{array}{ll} s_1 = \dfrac{1}{2} - \dfrac{3}{4}\xi + \dfrac{\xi^3}{4}, & s_2 = \dfrac{L}{8}\left(1 - \xi - \xi^2 + \xi^3\right), \\ s_3 = \dfrac{1}{2} + \dfrac{3}{4}\xi - \dfrac{\xi^3}{4}, & s_4 = \dfrac{L}{8}\left(-1 - \xi + \xi^2 + \xi^3\right) \end{array}\right\} \tag{2}$$

where, L is the length of the element and the dimensionless abscissa is defined as $\xi = 2\dfrac{x}{L} - 1$.

The constant mass matrix for the ANCF cable element is given by:

$$\mathbf{M} = \int_0^L \rho A \mathbf{S}^T \mathbf{S} dx \tag{3}$$

where, ρ is the density of the cable element, A is the cross section area of the beam and $\mathbf{S} = \left[s_1\mathbf{I} \quad s_2\mathbf{I} \quad s_3\mathbf{I} \quad s_4\mathbf{I} \right]$ is the matrix of shape functions. One of the major advantages of using ANCF is having a constant mass matrix and zero Coriolis and centrifugal effects. ANCF also assures continuity of slopes and rotations at nodes.

3.2 Catenary ANCF Finite Element Model

The ANCF catenary model used in this investigation is shown in the Fig. 4. A simple construction is used which consists of a messenger wire, a contact wire, supporting poles and droppers. The droppers are modeled as spring- damper elements with the physical properties of an actual dropper. The staggering of the messenger wire and the contact wire is neglected here for simplicity. The contact wire and the messenger wires are modeled using three-dimensional ANCF cable elements. The contact cable is modeled with the material properties of copper. As it is shown in Fig. 4, the catenary system has total 20 spans, each being 56.25 m in length. As discussed before, tensioning of the messenger and the contact cables has a significant impact on the contact force. The tension in the contact wire and the messenger wire is 20 kN and 14 kN respectively. To incorporate this tension force, equivalent nodal displacements are applied instead of direct nodal forces. A preliminary static equilibrium simulation is performed to obtain stable, straight configuration of the catenary system. Having obtained this equilibrium configuration, the dynamic simulations were performed with the full rail vehicle and the pantograph-catenary contact model.

The state of every dropper is checked before every integration time-step so as to determine whether it is in tension or compression. The dropper stiffness in compression is neglected. The nonlinear slackening effect of droppers is not being considered in this study. The general properties of the catenary computational model are shown in Table 3.

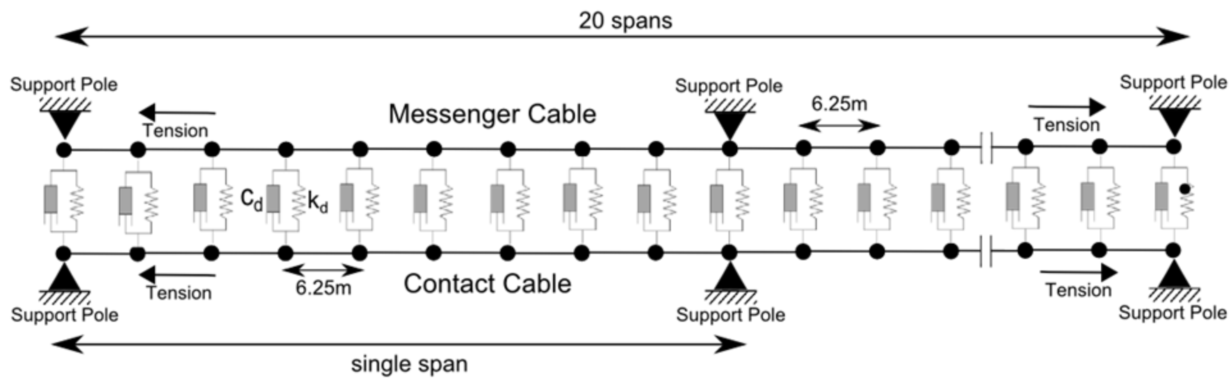

Figure 4. Catenary computational model (Pappalardo et al., 2015)

Table 4. Catenary Properties

Contact/Messenger Wire Geometry	
Elements per Span	9
Element Length (m)	6.25
Element Cross Section Area (mm^2)	144
Total Number of Spans	20
Catenary System Material Properties	
Contact Wire Density (kg/m^3)	8960
Contact Wire Modulus of Elasticity (Pa)	1.2E+11
Messenger Wire Modulus of Elasticity (Pa)	1.2E+11
Other General Catenary Properties	
Tension in Contact Wire (N)	20000
Tension in Messenger Wire (N)	14000
Dropper Stiffness k_d (N/m)	200000
Dropper Damping C_d (N/m)	10000

CHAPTER 4

GENERALIZED FORCES APPLIED ON THE PANTOGRAPH-CATENARY SYSTEM AND EQAUTIONS OF MOTION

This chapter discusses the different forces involved in the pantograph-catenary multibody model. These include the formulations for wheel/ rail contact, the new pantograph-catenary contact model, and the external aerodynamic forces. The equations of motion of the resulting rigid-flexible multibody system formed by the rail vehicle model, the pantograph mechanism and the catenary wires are described in this section as well.

4.1 Wheel/ Rail Contact Kinematics

A full rail vehicle is modeled on which the pantograph is mounted. This detailed rail vehicle model has a three dimensional non-conformal wheel/rail contact implemented. The contact point locations on the wheels and the rail are obtained by solving a set of following nonlinear algebraic equations- $\left(\mathbf{t}_1^r\right)^T\left(\mathbf{r}^w-\mathbf{r}^r\right)=\mathbf{0}$, $\left(\mathbf{t}_2^r\right)^T\left(\mathbf{r}^w-\mathbf{r}^r\right)=\mathbf{0}$, $\left(\mathbf{t}_1^w\right)^T\mathbf{n}^r=\mathbf{0}$, and $\left(\mathbf{t}_2^w\right)^T\mathbf{n}^r=\mathbf{0}$. The superscripts w and r stand for the wheel and the rail respectively, $\mathbf{r}^w$ and $\mathbf{r}^r$ are the global position vectors of the potential contact point on the wheel and rail respectively, $\mathbf{t}_1^w$ and $\mathbf{t}_2^w$ are the tangents to the wheel surface at the contact point, $\mathbf{n}^w$ is the normal to the wheel surface at the contact point, $\mathbf{t}_1^r$ and $\mathbf{t}_2^r$ are the two tangents to the rail, and $\mathbf{n}^r$ is the normal to the rail. The wheel and rail surface parameters are obtained after solving these equations. The solution of these equations also ensures that the coordinates of the contact point on the wheel and the rail surface are the same along the tangents $\mathbf{t}_1^r$ and $\mathbf{t}_2^r$. The tangent planes are at the contact point are the same for the wheel and the rail surfaces. The contact equations can be written in a vector form as:

$$\mathbf{C}^{w,r}\left(\mathbf{q}^r,\mathbf{q}^w,\mathbf{s}^r,\mathbf{s}^w,t\right)=\mathbf{0} \tag{4}$$

where $\mathbf{q}^r$ is the vector of generalized coordinates of the rail, $\mathbf{q}^w$ is the vector of generalized coordinates of the wheel, $\mathbf{s}^r$ is the vector of non-generalized coordinates or surface parameters of the rail, and $\mathbf{s}^w$ is the vector of non-generalized coordinates or surface parameters of the wheel. Given the vectors of the generalized coordinates of the wheel and rail $\mathbf{q}^w$ and $\mathbf{q}^r$, equation (4) can be solved for the surface parameters using an iterative Newton-Raphson method. The following equation is used for the Newton- Raphson iterations:

$$\left(\partial \mathbf{C}^{w,r} / \partial \mathbf{s}^w\right) \Delta \mathbf{s}^w + \left(\partial \mathbf{C}^{w,r} / \partial \mathbf{s}^r\right) \Delta \mathbf{s}^r = -\mathbf{C}^{w,r} \tag{5}$$

where, $\Delta \mathbf{s}^w$ and $\Delta \mathbf{s}^r$ are the Newton differences.

4.2 Pantograph/Catenary Elastic Contact Formulation

Accurate evaluation of the contact force between the pantograph and the catenary is very crucial, and a new contact formulation is proposed in this investigation based on the sliding joint formulation presented in the previous investigations (Seo et al., 2005; Seo et al., 2007; Pappalardo et al., 2015).

4.2.1 Contact Kinematics

The pantograph can lose contact with the contact wire under adverse conditions, and this can result into severe problems like arcing and potentially can damage the system components critically. Hence modeling the loss of contact is one of the important features of the elastic contact or the penalty approach which cannot be done using the sliding joint formulation. In the presented new contact formulation based on the elastic contact approach, the concept of non-generalized coordinates is used.

The constraint equations at the contact point P for the sliding joint are written as:

$$\left.\begin{aligned}\mathbf{C}^s &= \mathbf{C}^s(\mathbf{q}^p, \mathbf{e}^c, s, t)\\ \mathbf{C}^s &= \mathbf{r}^p - \mathbf{r}^c = \mathbf{0}\end{aligned}\right\} \tag{6}$$

where, $\mathbf{r}^p = \mathbf{r}^p(\mathbf{q}^p, t)$ is the global position vector of the contact point P on the pan-head, $\mathbf{r}^c = \mathbf{r}^c(\mathbf{e}^c, s, t)$ is the global position vector of the contact point P on the catenary, $\mathbf{q}^p = \mathbf{q}^p(t)$ is the vector of generalized coordinates of the pan-head, $\mathbf{e}^c = \mathbf{e}^c(t)$ is the vector of the nodal coordinates of the flexible ANCF contact cable, and $s = s(t)$ is the non-generalized coordinate which is used to define the location of the contact point on the contact wire. The sliding joint constraints can be also written in a different form using three unit vectors of a tangent frame defined on the catenary cable as follows,

$$\mathbf{C}^s = \begin{bmatrix} \left(\mathbf{i}_t^c\right)^T\left(\mathbf{r}^p - \mathbf{r}^c\right) \\ \left(\mathbf{j}_t^c\right)^T\left(\mathbf{r}^p - \mathbf{r}^c\right) \\ \left(\mathbf{k}_t^c\right)^T\left(\mathbf{r}^P - \mathbf{r}^c\right) \end{bmatrix} = \mathbf{0} \tag{7}$$

where, $\mathbf{i}_t^c = \mathbf{i}_t^c(\mathbf{e}^c, s, t)$, $\mathbf{j}_t^c = \mathbf{j}_t^c(\mathbf{e}^c, s, t)$ and $\mathbf{k}_t^c = \mathbf{k}_t^c(\mathbf{e}^c, s, t)$ are the three unit vectors of a tangent frame defined on the catenary cable at the contact point (Sugiyama et al., 2003). The new sliding joint formulation proposed by Pappalardo et al. uses only one gradient vector to define the constraint equations which can be applied to the gradient deficient ANCF elements, like the cable element, as well as the fully parameterized ANCF elements. The sliding joint formulation proposed by Seo et al. can be used for only fully parameterized elements. In general there are two approaches with which the contact problem can be solved, namely the augmented formulation and the embedding technique. The augmented formulation uses the constraint equations and the Lagrange multipliers to solve the system treating the non-generalized coordinates as degrees of freedom, whereas in embedding technique, the non-generalized coordinate, the arc length parameter, is systematically eliminated to solve for only two contact equations instead of three.

4.2.2 The New Contact Formulation

As shown in equation (7), three gradient vectors are needed to define the tangent frame, whereas in the formulation proposed by Pappalardo et al., only one gradient vector, $\mathbf{r}_x^c = \left[\left(\mathbf{r}_x^c\right)_1 \quad \left(\mathbf{r}_x^c\right)_2 \quad \left(\mathbf{r}_x^c\right)_3\right]^T$, is needed. The three unit vectors in equation (7) are replaced by the following three orthogonal vectors (Gere and Weaver, 1965; Shabana, 2013).

$$\mathbf{r}_x^c = \begin{bmatrix} \left(\mathbf{r}_x^c\right)_1 \\ \left(\mathbf{r}_x^c\right)_2 \\ \left(\mathbf{r}_x^c\right)_3 \end{bmatrix}, \quad \mathbf{n}_1^c = \begin{bmatrix} -\left(\mathbf{r}_x^c\right)_1\left(\mathbf{r}_x^c\right)_2 \\ \left(\left(\mathbf{r}_x^c\right)_1\right)^2 + \left(\left(\mathbf{r}_x^c\right)_3\right)^2 \\ -\left(\mathbf{r}_x^c\right)_2\left(\mathbf{r}_x^c\right)_3 \end{bmatrix}, \quad \mathbf{n}_2^c = \begin{bmatrix} -\left(\mathbf{r}_x^c\right)_3 \\ 0 \\ \left(\mathbf{r}_x^c\right)_1 \end{bmatrix} \tag{8}$$

This formulation of the vectors becomes singular if the vector $\mathbf{r}_x^c$ becomes parallel to the vector $\begin{bmatrix}0 & 1 & 0\end{bmatrix}^T$. In this case, the following three orthogonal vectors can be used,

$$\mathbf{r}_x^c = \begin{bmatrix} 0 \\ \left(\mathbf{r}_x^c\right)_2 \\ 0 \end{bmatrix}, \quad \mathbf{n}_1^c = \begin{bmatrix} -\left(\mathbf{r}_x^c\right)_2 \\ 0 \\ 0 \end{bmatrix}, \quad \mathbf{n}_2^c = \begin{bmatrix} 0 \\ 0 \\ 1 \end{bmatrix} \tag{9}$$

With the help of these orthogonal vectors, the equation (7) of contact constraints can be rewritten as,

$$\mathbf{C}^s = \begin{bmatrix} \left(\mathbf{r}^c - \mathbf{r}^p\right)^T \mathbf{r}_x^c \\ \left(\mathbf{r}^c - \mathbf{r}^p\right)^T \mathbf{n}_1^c \\ \left(\mathbf{r}^c - \mathbf{r}^p\right)^T \mathbf{n}_2^c \end{bmatrix} = \mathbf{0} \tag{10}$$

These algebraic constraint equation are function of a single gradient vector, $\mathbf{r}_x^c$. For the ANCF finite elements, the spatial coordinate x can always be expressed as a function of the arc length non-generalized parameter s, that is $x = x(s)$. Therefore $\mathbf{r}_s^c$ is a vector parallel to the vector $\mathbf{r}_x^c$, implying that any of these can be used to formulate the contact constraints. In the elastic contact formulation proposed, the first constraint equation is used to eliminate the arc length parameter, and the other two equations, referred as $\mathbf{C}_m^s = \mathbf{0}$, are imposed using a penalty formulation which produces a unilateral force.

The arc length parameter is eliminated by applying Newton- Raphson iterative method to the first constraint equation, $C_e^s = \left(\mathbf{r}^c - \mathbf{r}^p\right)^T \mathbf{r}_x^c = 0$, as follows. The equation used in the Newton-Raphson algorithm is $\left(C_e^s\right)_s \Delta s = -C_e^s$, where $\left(C_e^s\right)_s = \partial C_e^s / \partial s$ and Δs is the Newton difference. It can be shown that $\left(C_e^s\right)_s = \partial C_e^s / \partial s = \left(\partial \mathbf{r}^c / \partial s\right)^T \mathbf{r}_x^c + \mathbf{r}^{cpT}\left(\partial \mathbf{r}_x^c / \partial s\right)$, where $\mathbf{r}^{cp} = \mathbf{r}^c - \mathbf{r}^p$. A necessary condition to eliminate the arc length s is that the term $\left(C_e^s\right)_s$ has to be non-zero, and the simplicity of the catenary geometry will ensure satisfaction of this condition.

The other two constraints $\mathbf{C}_m^s = \mathbf{0}$ are imposed using the penalty method, hence the Jacobian matrix for these constraints is needed. The first constraint equation gives, $\left(C_e^s\right)_{\mathbf{q}} \delta\mathbf{q} + \left(C_e^s\right)_s \delta s = 0$, where $\mathbf{q} = \begin{bmatrix} \mathbf{e}^T & \mathbf{q}^{pT} \end{bmatrix}^T$ is the vector of generalized coordinates for the pan head and the contact wire, $\left(C_e^s\right)_{\mathbf{q}} = \partial C_e^s / \partial \mathbf{q} = \begin{bmatrix} \partial C_e^s / \partial \mathbf{e} & \partial C_e^s / \partial \mathbf{q}^p \end{bmatrix}$ is the Jacobian matrix associated with the vector of generalized coordinates $\mathbf{q}$, and $\left(C_e^s\right)_s = \partial C_e^s / \partial s = \mathbf{r}^{cpT}\mathbf{r}_{xs}^c + \mathbf{r}_x^{cT}\mathbf{r}_s^c$ is the Jacobian matrix associated with the arc length parameter s. The pan-head being a rigid body,

$$\left(C_e^s\right)_{\mathbf{q}} = \left[\partial C_e^s/\partial \mathbf{e} \quad \partial C_e^s/\partial \mathbf{q}^p\right] = \left[\left(\mathbf{r}^{cp^T}\mathbf{S}_x + \mathbf{r}_x^{cT}\mathbf{S}\right) \quad -\mathbf{r}_x^{cT}\mathbf{L}^p\right] \tag{11}$$

where, $\mathbf{L}^p = \partial \mathbf{r}^p/\partial \mathbf{q}^p = \left[\partial \mathbf{r}^p/\partial \mathbf{R}^p \quad \partial \mathbf{r}^p/\partial \boldsymbol{\theta}^p\right] = \left[\mathbf{I} \quad -\mathbf{A}^p\tilde{\bar{\mathbf{u}}}^p\bar{\mathbf{G}}^p\right]$, $\mathbf{I}$ is a 3×3 identity matrix, $\mathbf{q}^p = \left[\mathbf{R}^{pT} \quad \boldsymbol{\theta}^{pT}\right]^T$ is the is vector of generalized coordinates for the pan-head, $\mathbf{R}^p$ being the global position vector and $\boldsymbol{\theta}^p$ being the orientation parameters used to define the pan-head orientation, $\mathbf{A}^p$ is the transformation matrix defining the orientation of the local coordinate system of the pan-head, $\tilde{\bar{\mathbf{u}}}^p$ is the skew symmetric matrix associated with the vector $\bar{\mathbf{u}}^p$ that defines the location of the contact point on the pan-head with respect to the local coordinate system, and $\bar{\mathbf{G}}^p$ is the matrix that relates the angular velocity vector $\bar{\boldsymbol{\omega}}^p$ defined in the local coordinate system to the time derivatives of the pan-head orientation coordinates $\dot{\boldsymbol{\theta}}^p$, that is $\bar{\boldsymbol{\omega}}^p = \bar{\mathbf{G}}^p\dot{\boldsymbol{\theta}}^p$. It is evident that:

$$\delta s = -\left(\frac{\left(C_e^s\right)_{\mathbf{q}}}{\left(C_e^s\right)_s}\right)\delta\mathbf{q}, \quad \dot{s} = -\left(\frac{\left(C_e^s\right)_{\mathbf{q}}}{\left(C_e^s\right)_s}\right)\dot{\mathbf{q}} \tag{12}$$

For the last two constraint equations in the equation (10), a virtual change in the coordinates gives $\delta\mathbf{C}_m^s = \left(\mathbf{C}_m^s\right)_{\mathbf{q}}\delta\mathbf{q} + \left(\mathbf{C}_m^s\right)_s\delta s = \mathbf{0}$, and hence these constraints can be written at the velocity level as $\dot{\mathbf{C}}_m^s = \left(\mathbf{C}_m^s\right)_{\mathbf{q}}\dot{\mathbf{q}} + \left(\mathbf{C}_m^s\right)_s\dot{s} = \mathbf{0}$. Using equation (12), one can show that:

$$\left.\begin{aligned}
\delta\mathbf{C}_m^s &= \left(\left(\mathbf{C}_m^s\right)_{\mathbf{q}} - \frac{1}{\left(C_e^s\right)_s}\left(\mathbf{C}_m^s\right)_s\left(C_e^s\right)_{\mathbf{q}}\right)\delta\mathbf{q} = \mathbf{0} \\
\dot{\mathbf{C}}_m^s &= \left(\left(\mathbf{C}_m^s\right)_{\mathbf{q}} - \frac{1}{\left(C_e^s\right)_s}\left(\mathbf{C}_m^s\right)_s\left(C_e^s\right)_{\mathbf{q}}\right)\dot{\mathbf{q}} = \mathbf{0}
\end{aligned}\right\} \tag{13}$$

In order to eliminate the non-generalized arc length parameter s from the Jacobian matrix of the constraint equations, they are modified as follows,

$$\left.\begin{aligned}
&\left(C_e^s\right)_{\mathbf{q}} = \left[\left(C_e^s\right)_{\mathbf{e}^c} \quad \left(C_e^s\right)_{\mathbf{q}^p}\right] = \left[\mathbf{r}^{cpT}\left(\frac{\partial \mathbf{r}_x^c}{\partial \mathbf{e}^c}\right) + \mathbf{r}_x^{cT}\left(\frac{\partial \mathbf{r}^c}{\partial \mathbf{e}^c}\right) \quad -\mathbf{r}_x^{cT}\left(\frac{\partial \mathbf{r}^p}{\partial \mathbf{q}^p}\right)\right]\\
&\left(\mathbf{C}_m^s\right)_{\mathbf{q}} = \left[\left(\mathbf{C}_m^s\right)_{\mathbf{e}} \quad \left(\mathbf{C}_m^s\right)_{\mathbf{q}^p}\right] = \begin{bmatrix} \mathbf{r}^{cpT}\left(\dfrac{\partial \mathbf{n}_1^c}{\partial \mathbf{e}}\right) + \mathbf{n}_1^{cT}\left(\dfrac{\partial \mathbf{r}^c}{\partial \mathbf{e}}\right) & -\mathbf{n}_1^{cT}\left(\dfrac{\partial \mathbf{r}^p}{\partial \mathbf{q}^p}\right) \\ \mathbf{r}^{cpT}\left(\dfrac{\partial \mathbf{n}_2^c}{\partial \mathbf{e}}\right) + \mathbf{n}_2^{cT}\left(\dfrac{\partial \mathbf{r}^c}{\partial \mathbf{e}}\right) & -\mathbf{n}_2^{cT}\left(\dfrac{\partial \mathbf{r}^p}{\partial \mathbf{q}^p}\right) \end{bmatrix}\\
&\left(\mathbf{C}_m^s\right)_s = \begin{bmatrix} \left(\partial \mathbf{r}^c / \partial s\right)^T \mathbf{n}_1^c + \mathbf{r}^{cpT}\left(\partial \mathbf{n}_1^c / \partial s\right) \\ \left(\partial \mathbf{r}^c / \partial s\right)^T \mathbf{n}_2^c + \mathbf{r}^{cpT}\left(\partial \mathbf{n}_2^c / \partial s\right) \end{bmatrix}
\end{aligned}\right\} \tag{14}$$

The vectors $\partial \mathbf{r}^c / \partial \mathbf{e}$, $\partial \mathbf{r}^c / \partial s$ and $\partial \mathbf{r}_x^c / \partial \mathbf{e}$ can be written in terms of the catenary shape functions and their derivatives along with $\partial x / \partial s$. The partial derivatives of the vectors $\mathbf{n}_1^c$ and $\mathbf{n}_2^c$ with respect to $\mathbf{e}$ and s can be written as,

$$\left.\begin{aligned}
\partial \mathbf{n}_1^c / \partial \mathbf{e} &= \mathbf{H}_1^c\left(\partial \mathbf{r}_x^c / \partial \mathbf{e}\right)\\
\partial \mathbf{n}_1^c / \partial s &= \mathbf{H}_1^c\left(\partial \mathbf{r}_x^c / \partial s\right)\\
\partial \mathbf{n}_2^c / \partial \mathbf{e} &= \mathbf{H}_2^c\left(\partial \mathbf{r}_x^c / \partial \mathbf{e}\right)\\
\partial \mathbf{n}_2^c / \partial s &= \mathbf{H}_2^c\left(\partial \mathbf{r}_x^c / \partial s\right)
\end{aligned}\right\} \tag{15}$$

where,

$$\mathbf{H}_1^c = \begin{bmatrix} -\left(\mathbf{r}_x^c\right)_2 & -\left(\mathbf{r}_x^c\right)_1 & 0 \\ 2\left(\mathbf{r}_x^c\right)_1 & 0 & 2\left(\mathbf{r}_x^c\right)_3 \\ 0 & -\left(\mathbf{r}_x^c\right)_3 & -\left(\mathbf{r}_x^c\right)_2 \end{bmatrix}, \quad \mathbf{H}_2^c = \begin{bmatrix} 0 & 0 & -1 \\ 0 & 0 & 0 \\ 1 & 0 & 0 \end{bmatrix} \tag{16}$$

Having evaluated the Jacobian matrices of the constraint equations and having eliminated the arc length parameter, the last two constraint equations $\mathbf{C}_m^s = \mathbf{0}$ can be imposed using the penalty force, $\mathbf{Q}_{Penalty}$, formulation which is given as:

$$\mathbf{Q}_{Penalty} = -k\left(\bar{\mathbf{C}}_{\mathbf{q}}\right)^T\left(\mathbf{C}_m^s\right) - d\left(\bar{\mathbf{C}}_{\mathbf{q}}\right)^T\left(\dot{\mathbf{C}}_m^s\right) \tag{17}$$

where, k is the penalty stiffness coefficient, d is the penalty damping coefficient, the Jacobian matrix of the constraints $\bar{\mathbf{C}}_{\mathbf{q}}$ is given by $\bar{\mathbf{C}}_{\mathbf{q}} = \left(\mathbf{C}_m^s\right)_{\mathbf{q}} - \left(\left(\mathbf{C}_m^s\right)_s \left(C_e^s\right)_{\mathbf{q}}\right) \Big/ \left(C_e^s\right)_s$ and the derivatives of the constraints $\dot{\mathbf{C}}_m^s$ can be obtained as written in equation (13). This computed penalty force is applied as an external force on the contact wire and the pan-head at the point of contact.

4.2.3 Contact Force Regulations

The required quality standards for the contact force in the pantograph-catenary interaction in high- speed trains are specified in current regulations (EN50317, 2012; EN50367, 2006). In this investigation, the norm EN50367 is referred. It specifies following parameters for the pantograph acceptance:

- Mean Contact Force: $F_m = 0.00097v^2 + 70\text{N}$, where v represents the velocity of the train;
- Standard Deviation: $\sigma_{max} < 0.3F_m$;

- Maximum Contact Force: $F_{max} < 350\,\text{N}$

- Maximum Catenary Wire Uplift at Steady Arm: $d_{up} \leq 120\,\text{mm}$

- Maximum Pantograph Vertical Amplitude: $\Delta_z \leq 80\,\text{mm}$

- Percentage of Real Arcing: $NQ \leq 0.2\%$

All of the above parameters are considered here, except for percentage of real arcing parameter.

4.3 Aerodynamic Forces

The effect of aerodynamic forces has to be considered while designing the pantograph as they have a significant impact on the mean contact force value. The drag and the lift force components of the cross-wind tend to add to the uplift force exerted on the pantograph mechanism (Pombo et al., 2009). This effect is referred to as the aerodynamic uplift. For the pantographs having multiple pan-heads, an imbalance might be introduced due to the aerodynamic forces causing one of the collector strips to wear faster than the other (Bacciolone et al., 2006; Carnevale et al., 2015; Pombo et al., 2009). The turbulence created in the boundary layer close to the car body roof due to vortex shedding can excite the pantograph components affecting the current collection quality. The vortex shedding at the pan-head wake may generate high frequencies and the sparking level can increase significantly (Bacciolone et al., 2006; Ikeda et al., 2009). Therefore, it becomes essential to account for the aerodynamic forces while simulating the pantograph-catenary systems.

A new approach is used in this investigation so as to apply the time varying nonlinear aerodynamic forces on individual components of the pantograph and the flexible ANCF catenary as well. The approximate drag and the lift coefficients for the individual pantograph components are obtained from the previous experimental and numerical studies regarding the influence of the aerodynamic forces on the pantograph-catenary interaction (Carnevale et al., 2015; Pombo et al., 2009). The aerodynamic pressure coefficients are basically the force exerted by the drag and the lift component per unit of the kinetic energy of the wind flow. The values used of these coefficients are shown in Table 5. The effect of aerodynamic pitching moment is not considered in this study. In order to compute the aerodynamic forces on each body, a set of material points distributed on different locations on each body is considered. This provision is made so that the aerodynamic forces would be properly distributed. In the computer implementation of the aerodynamic forces, the aerodynamic mesh created from these markers is read from a user-written external data file. The data file contains thirteen parameters for each marker created, which includes three Cartesian position coordinates with respect to the body coordinate system, nine direction cosines defining the orientation of the marker with respect to the body coordinate system and the area corresponding to the marker. Since aerodynamic pressure coefficients are used in this study, the area can be simply considered as one for each marker. In the case of flexible catenary, the nodal locations are used to define the marker data. The user also defines the aerodynamic coefficients for drag and lift, the density of the fluid and the wind velocity. A streamlined wind flow is considered in this case. The relative velocity between the body on which aerodynamic forces are to be applied and the wind is computed at each integration time-step. The lift and the drag forces on a body are then calculated using equation (18). The direction of these forces depends on the direction of the relative velocity as shown in Fig. 5.

$$\left.\begin{aligned}\mathbf{F}_D &= \left(\frac{1}{2}\rho\left(C_D A\right)\left|\mathbf{v}_r\right|^2\right)\hat{\mathbf{v}}_r \\ \mathbf{F}_L &= \left(\frac{1}{2}\rho\left(C_L A\right)\left|\mathbf{v}_r\right|^2\right)\hat{\mathbf{v}}_L\end{aligned}\right\} \tag{18}$$

In equation (18), $\mathbf{F}_D$ and $\mathbf{F}_L$ are the drag and the lift forces respectively, ρ is the density of the fluid, $(C_D A)$ and $(C_L A)$ are the drag and the lift pressure coefficients respectively, $\mathbf{v}_r$ is the relative velocity vector between the velocity of the body and the wind velocity and $\hat{\mathbf{v}}_r$ and $\hat{\mathbf{v}}_L$ being the unit vectors in the direction of the drag and the lift forces respectively.

Table 5. Aerodynamics coefficients for the pantograph components

Pantograph Component	**Drag Coefficient** $(C_D A)$	**Lift Coefficient** $(C_L A)$
Lower Arm	0.007	-0.0075
Lower Link	0.008	-0.001
Upper Arm	0.07	0.02
Pan-head	0.05	0.02

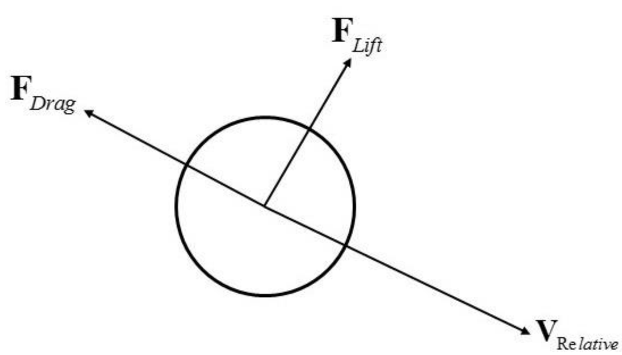

Figure 5. The direction of the drag and the lift forces

4.4 Equations of Motion of a Multibody System

The equations of motion for a general multibody system consisting of rigid bodies and very flexible bodies subjected to a set of kinematic constraints and external forces can be given by equation (19). The vector of generalized coordinates for the system can be given as, $\mathbf{p} = \begin{bmatrix} \mathbf{q}_r^T & \mathbf{e}^T & \mathbf{s}^T \end{bmatrix}^T$ where $\mathbf{q}_r$ defines the reference coordinates of the bodies, $\mathbf{e}$ defines the vector of coordinates for the flexible bodies subjected to large deformations, and $\mathbf{s}$ defines the vector of non-generalized coordinates or surface parameters used in the contact formulations. The equations of motion given in equation (19) are constructed using the augmented Lagrangian formulation.

$$\begin{bmatrix} \mathbf{M}_{rr} & \mathbf{0} & \mathbf{0} & \mathbf{C}_{q_r}^T \\ \mathbf{0} & \mathbf{M}_{ee} & \mathbf{0} & \mathbf{C}_e^T \\ \mathbf{0} & \mathbf{0} & \mathbf{0} & \mathbf{C}_s^T \\ \mathbf{C}_{q_r} & \mathbf{C}_e & \mathbf{C}_s & \mathbf{0} \end{bmatrix} \begin{bmatrix} \ddot{\mathbf{q}}_r \\ \ddot{\mathbf{e}} \\ \ddot{\mathbf{s}} \\ \boldsymbol{\lambda} \end{bmatrix} = \begin{bmatrix} \mathbf{Q}_r \\ \mathbf{Q}_e \\ \mathbf{0} \\ \mathbf{Q}_c \end{bmatrix} \tag{19}$$

In equation (19), $\boldsymbol{\lambda}$ is the vector of Lagrange multipliers, $\mathbf{M}_{rr}$ is the mass matrix associated with the reference motion of the bodies, $\mathbf{M}_{ee}$ is the mass matrix of the ANCF finite elements, $\mathbf{C}_{\mathbf{q}_r}$ and $\mathbf{C}_e$ are the constraint Jacobian matrices associated with the coordinates $\mathbf{q}_r$ and $\mathbf{e}$, respectively. The generalized forces associated with these coordinates are given by $\mathbf{Q}_r$ and $\mathbf{Q}_e$, respectively. $\mathbf{Q}_c$ is a quadratic velocity vector which results from the differentiation of the constraint equations twice with respect to time (Shabana, 2013).

CHAPTER 5

NUMERICAL RESULTS AND DISCUSSION

The numerical results obtained from the newly proposed contact model are presented in this section. The penalty force based contact formulation can be used with the fully parameterized ANCF finite elements and also with the gradient deficient elements. The gradient deficient cable element has been used in this investigation so as to achieve more efficient simulation times and also to avoid locking problems pertaining to the fully parameterized elements. The effect of the aerodynamic forces on the contact force is evaluated as well. Cross wind loading conditions are applied on both, the pantograph and the catenary system.

5.1 Without Wind Loading

In this subsection, the simulation results for the case where no wind loading is considered on the pantograph-catenary system are presented. A multibody model representing Faiveley CX pantograph is used in this investigation. The rail- vehicle is travelling at a velocity of 200 km/h on a straight track with no wind action on neither the pantograph nor the catenary system. A simulation span of 10 seconds is considered for the analysis. The uplift force exerted on the pantograph mechanism is modeled as a vertically upward force applied on the lower arm having a value of 1465 N.

The contact force evolution with time is presented in Fig. 6. Figure 7 shows the zoomed version of the results in Fig. 6 in the time window of 7 to 10 seconds. Boundary effects in the catenary model are evident in the initial simulation time. As observed in Fig. 6, in the timeframe from 1 to 2 seconds, the transverse waves are dominant in the catenary system and approximately after 2 seconds they attenuate. The contact force behavior this point onwards is mostly periodic denoting a steady state of operation. Hence in the analysis of the contact force, the first two seconds of numerical data is not considered till the system achieves a steady state. Figure 7 shows large peaks of the contact when the pantograph passes under a support pole positions and the droppers. The peaks corresponding to the support poles are much higher than the droppers.

A comparative plot is shown in Fig. 8 between the contact force results obtained from the sliding joint formulation proposed by Papplardo et al. and the new penalty formulation proposed in this investigation. The numerical results for the contact force in the case where no control action is employed with the contact force are considered from Pappalardo et al. (2015) for the comparison. Fig. 9 shows a good agreement between the contact force obtained using the constraint-based formulation and the penalty approach. The mean contact force for the penalty force formulation comes out to be -107.79 N against -110.427 N that of sliding joint formulation. The standard deviation of the contact force computed with the penalty force formulation is found to be 36.7257 N, where the sliding joint formulation contact force has a standard deviation of 37.3033 N. The mean contact force and the standard deviation of the contact force are within the limits prescribed by the standard EN50367, which are discussed before.

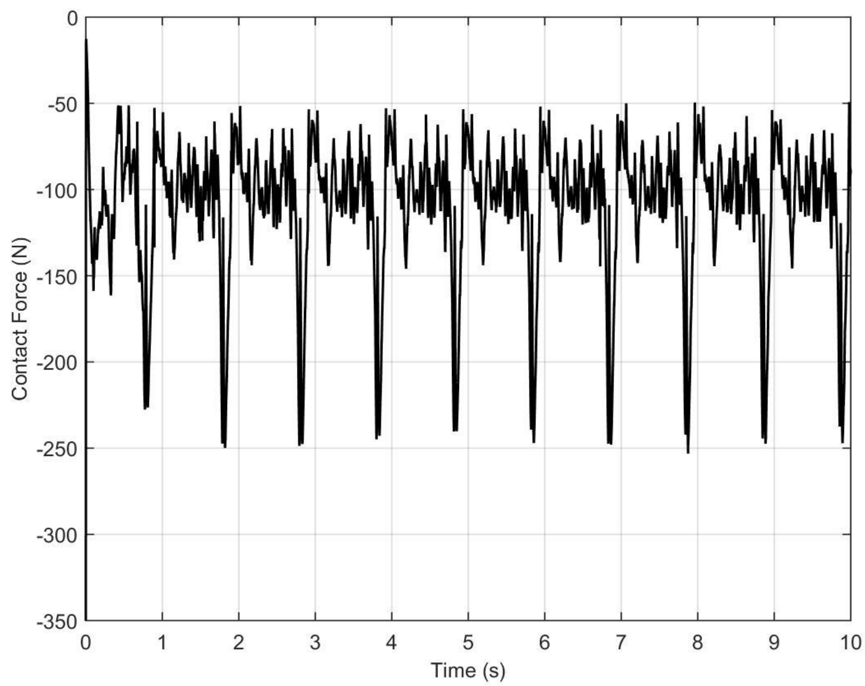

Figure 6. Contact force without wind loading

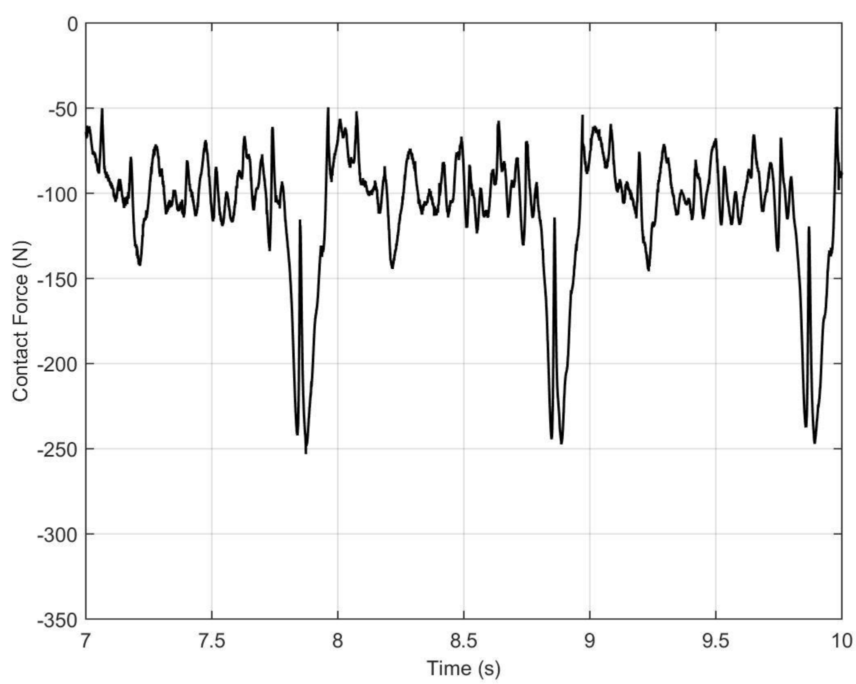

Figure 7. Contact force without wind loading- zoomed window

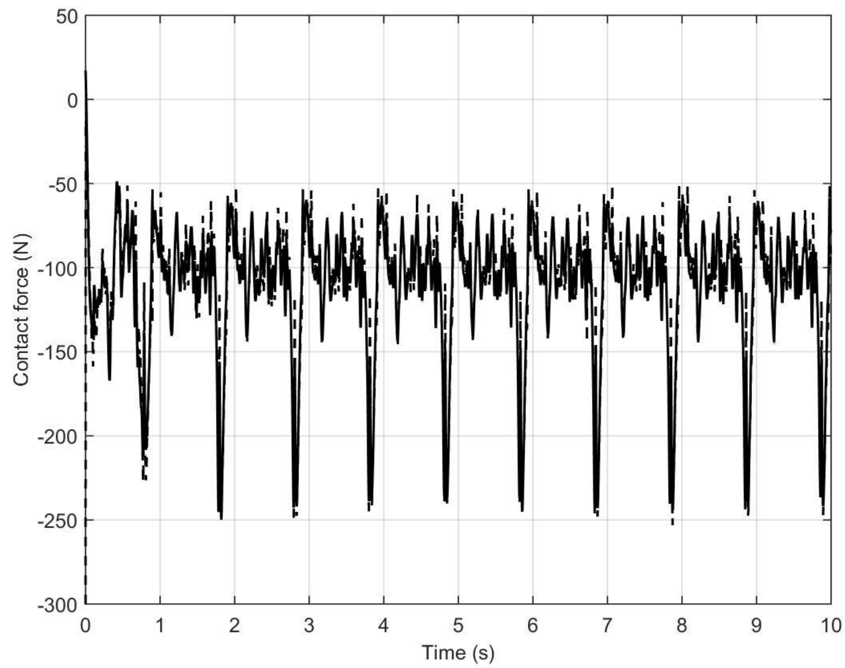

Figure 8. Contact force comparison between the sliding joint formulation and the penalty formulation (– – – Penalty Force Formulation, —— Sliding Joint Formulation)

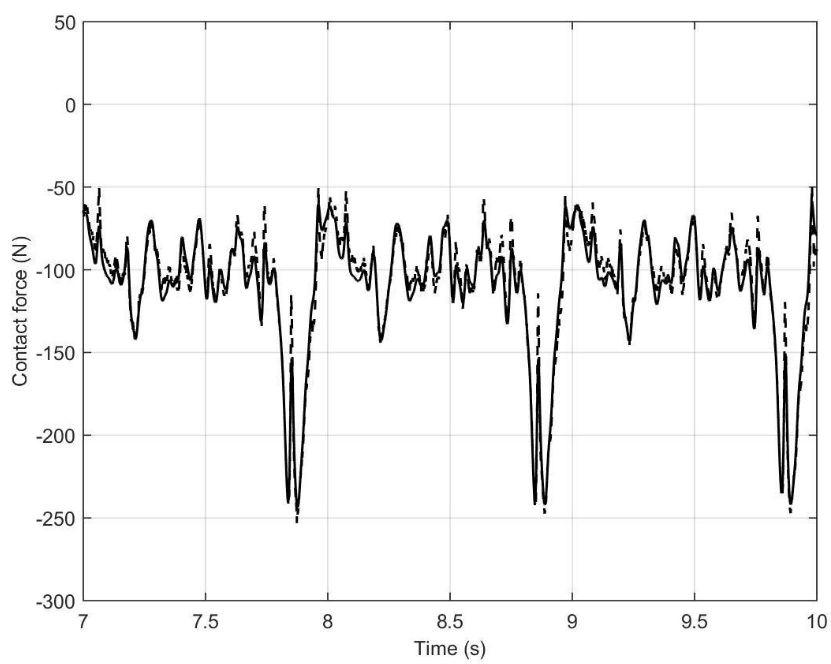

Figure 9. Contact force comparison between the sliding joint formulation and the penalty formulation- zoomed window (– – – Penalty Formulation, —— Sliding Joint Formulation)

5.2 With Wind Loading

The effect of the aerodynamic forces on the contact force is discussed in this section. The rail-vehicle velocity of 200 km/h and the uplift force on the pantograph mechanism of 1465 N are kept the same as that of the case where wind loading is not considered. There are two cases considered here; the first being a crosswind loading applied on the pantograph components only and the second being crosswind load being applied on the pantograph and the catenary system as well. In both, the case the wind having velocity of 20 m/s at a yaw angle of 15 degrees is considered. The wind flow is assumed to be streamlined, i.e. without any turbulence.

Figure 10 shows the plot of the contact force when the crosswind is applied only on the pantograph components. The aerodynamic forces are applied mainly on the four components of the pantograph which contribute to the total aerodynamic uplift force significantly, these components are- upper arm, lower arm, lower link and pan-head. These components are shown in Figure 2. The aerodynamic forces are applied at the center of gravity for each component. The aerodynamic pressure coefficients of drag and lift used are mentioned in Table 4. These coefficients are not dependent on the Reynolds number, which is confirmed by the trial tests mentioned in the standard EN50317. The standard states that the aerodynamic uplift force depends on the square of train velocity (Pombo et al., 2009). The effect of the aerodynamic pitching moment is not considered in this investigation. The time evolution of the drag and the lift force on the pan-head is shown in the Fig. 11 and Fig. 12, respectively. The drag and the lift forces are nonlinear in nature and are dependent on the velocity of the train and the wind loading conditions. The positive lift force indicates that the pan-head is lifted upwards causing an increase in the mean contact force. This effect can be observed from Figure 13 and Figure 14, where comparison in the contact force results is made between the case where crosswind is applied and the case where no wind loading is present. However, the effect of pan-head being lifted upwards depends on a lot of parameters like the collector geometry profile, usage of spoilers, turbulence in wind etc. The mean contact force in the case of crosswinds applied on the pantograph is found to be -120.22 N where it is -107.79 N when there is no wind, which is a 11.53% increase. The standard deviations are found to be similar in both the cases. However, the turbulence in the wind can have some effect on the standard deviation of the contact force.

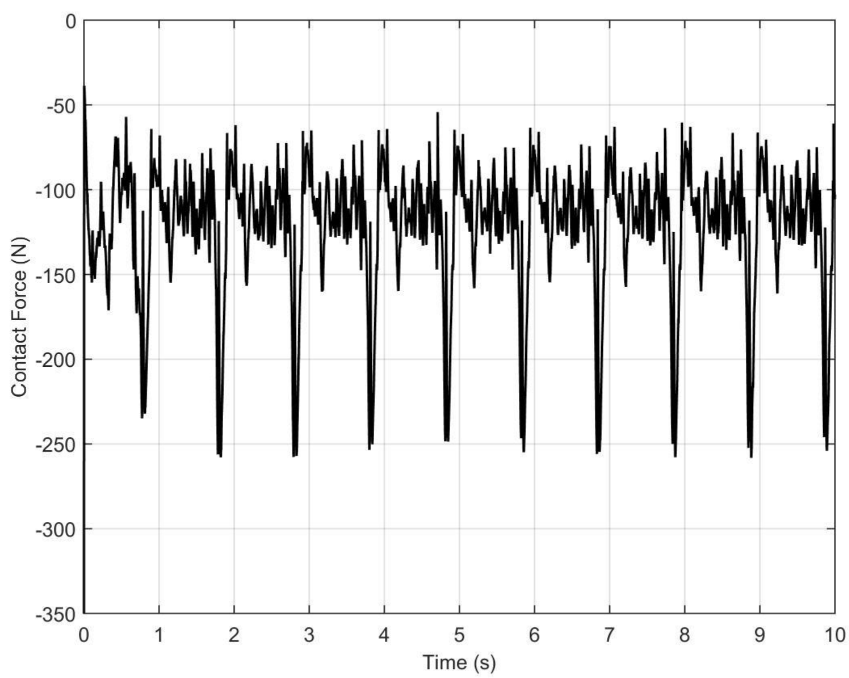

Figure 10. Contact force with cross wind loading on the pantograph components of 20 m/s at a yaw angle of 15 degrees

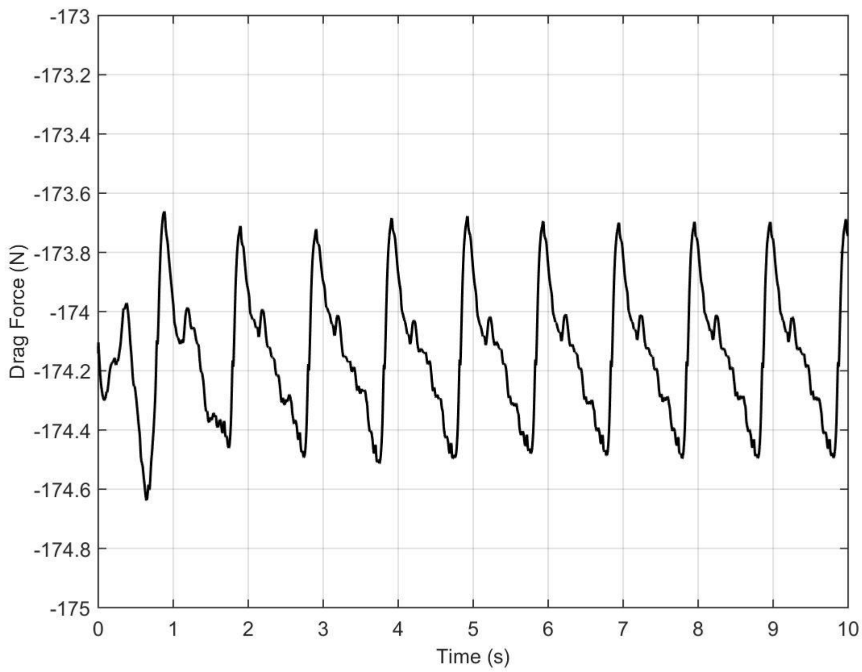

Figure 11. Drag force on the pan-head

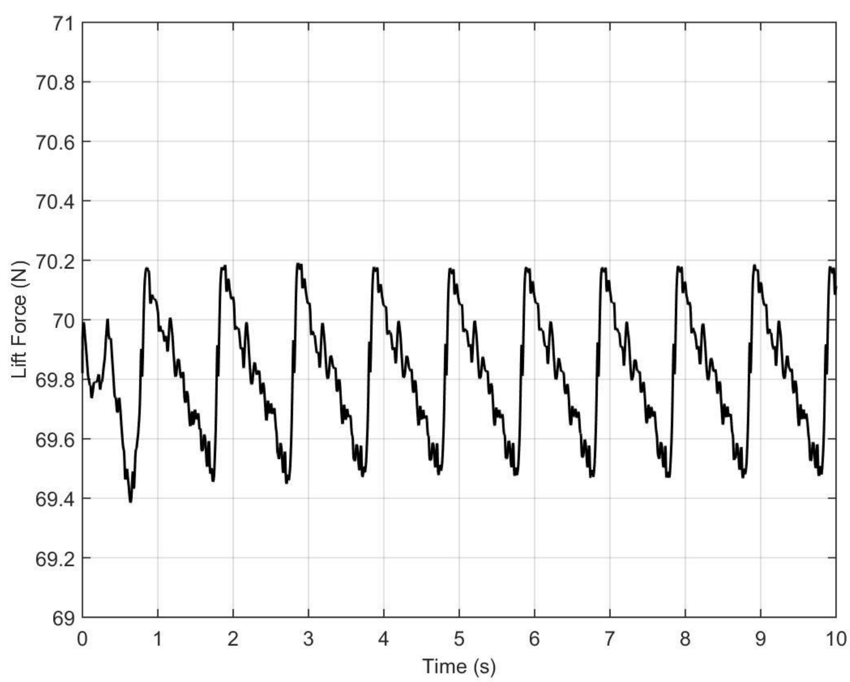

Figure 12. Lift force on the pan-head

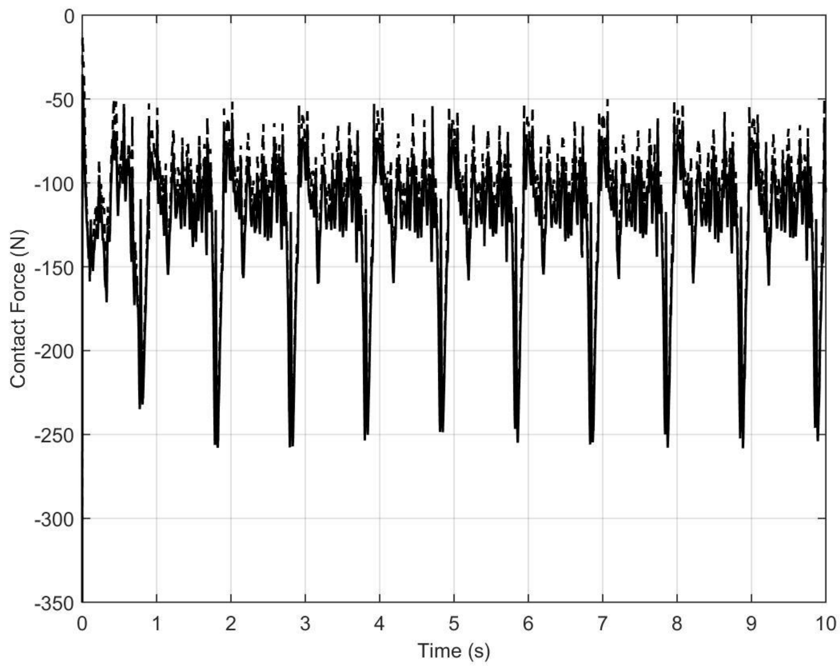

Figure 13. Contact force comparison with crosswind loading on the pantograph components of 20 m/s at a yaw angle of 15 degrees and with no wind loading (– – – Without wind loading, —— With crosswind loading)

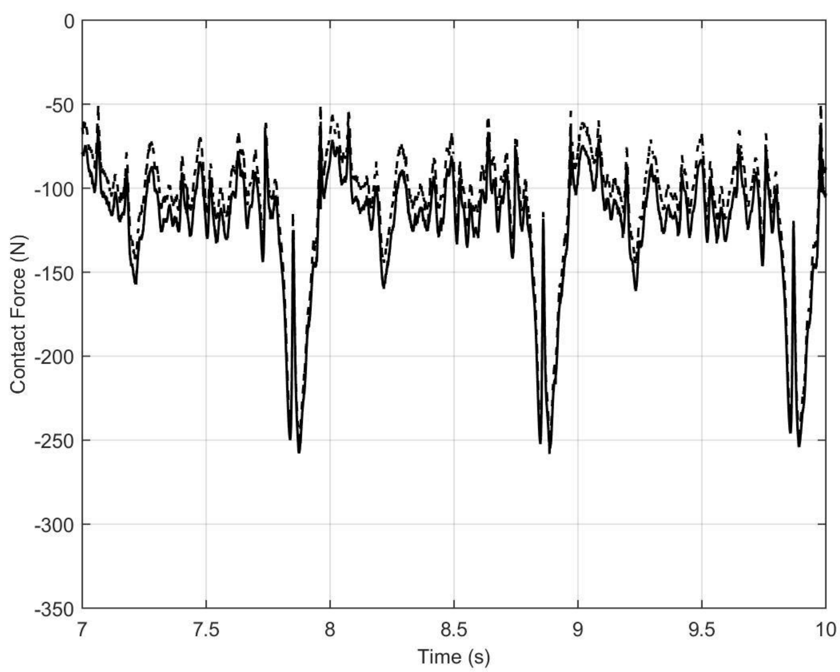

Figure 14. Contact force comparison with crosswind loading on the pantograph components of 20 m/s at a yaw angle of 15 degrees and with no wind loading- zoomed window (– – – Without wind loading, —— With crosswind loading)

Figure 15 shows the numerical results for the contact force for the case where the aerodynamic forces are applied on the pantograph components and also the catenary system. The aerodynamic forces are applied on both, the contact wire and the messenger wire as well. The mean contact force and the standard deviation of the contact force values are -120.21 N and 35.66 N respectively. Figure 16 and 17 compare the contact force numerical results obtained from applying the wind forces on the pantograph components and the catenary and the case where no aerodynamic forces are present. As reported in Table 5, there is an increase of 11.53% in the mean contact force value and a decrease of 2.91% in the standard deviation of the contact force. It can be observed that, these values are similar to those obtained by applying the aerodynamic forces only on the pantograph components. Hence the effect of aerodynamic forces applied on the catenary seems to be negligible for the considered wind conditions and the catenary configuration. Table 5 shows the values for the mean contact force and standard deviation for all the cases considered above.

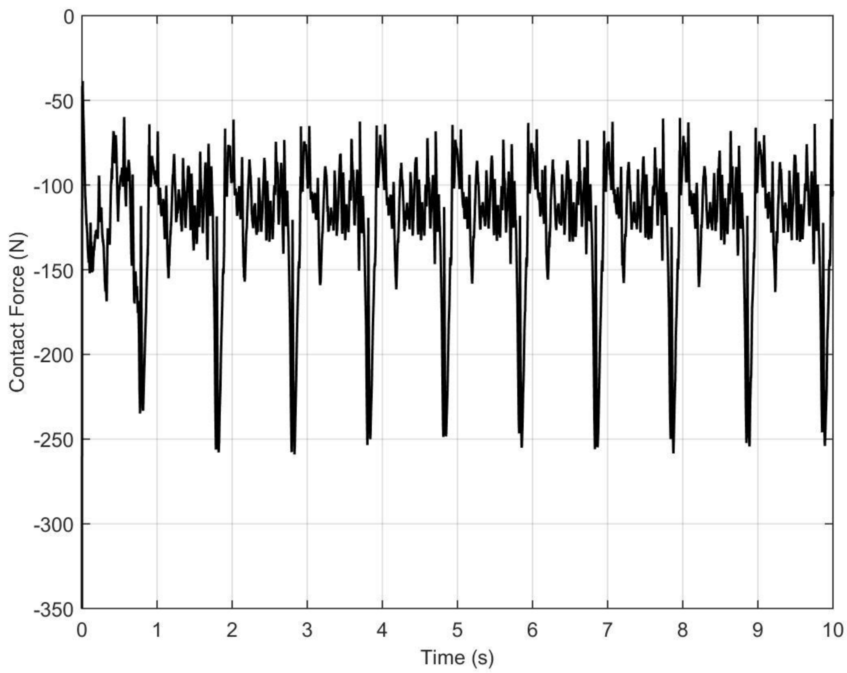

Figure 15. Contact force with cross wind loading on the pantograph components and the catenary of 20 m/s at a yaw angle of 15 degrees

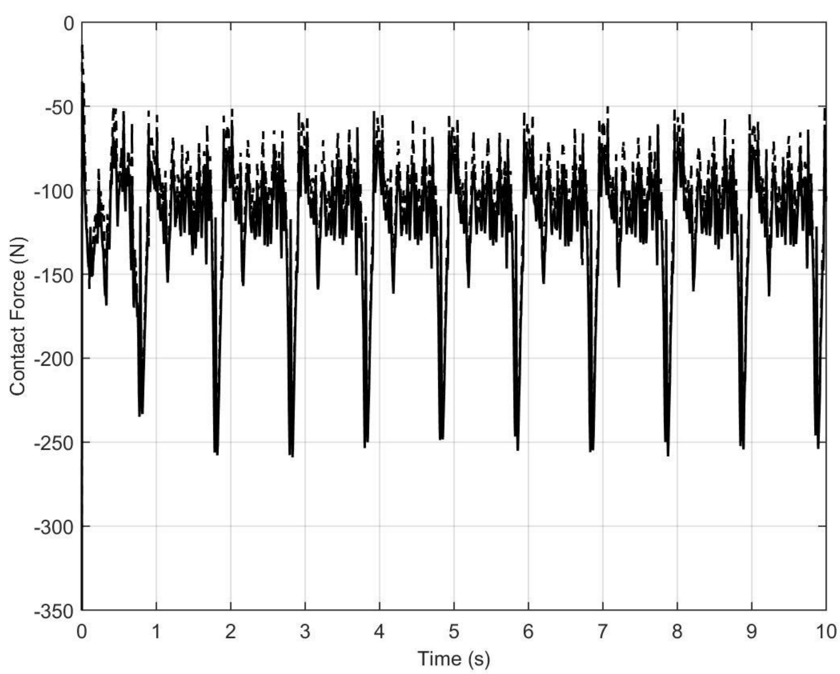

Figure 16. Contact force comparison with crosswind loading on the pantograph components and the catenary of 20 m/s at a yaw angle of 15 degrees and with no wind loading (– – – Without wind loading, —— With crosswind loading)

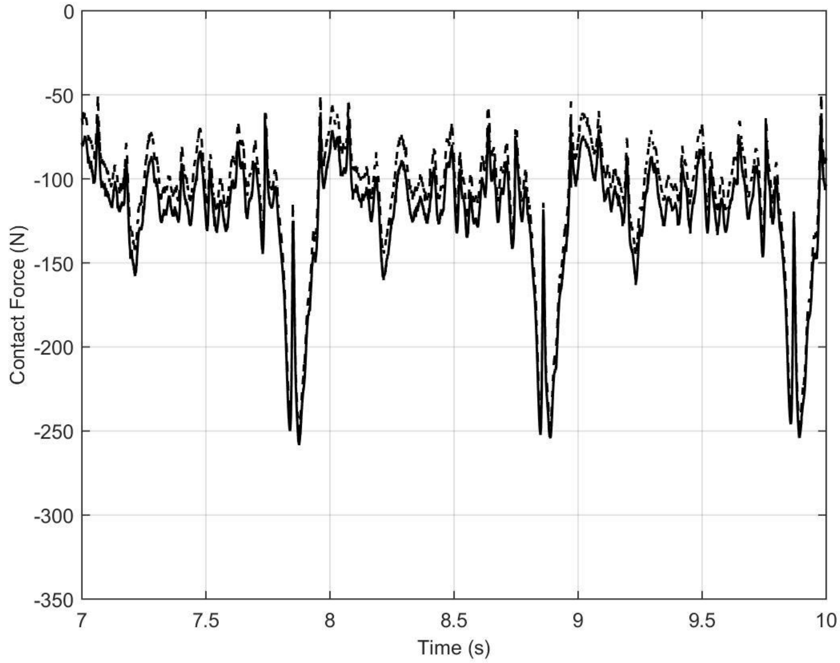

Figure 17. Contact force comparison with crosswind loading on the pantograph components and the catenary of 20 m/s at a yaw angle of 15 degrees and with no wind loading- zoomed window (– – – Without wind loading, —— With crosswind loading)

Table 6: Numerical results for the contact force mean value and the standard deviation in the contact force

Wind Loading	**Mean Force** (N)	**Std. Dev** (N)	**∆ Mean Force**	**∆ Force Std. Dev**
No wind	-107.79	36.73	/	/
Wind only on the pantograph	-120.22	35.70	11.53%	-2.80%
Wind on the pantograph and the catenary	-120.21	35.66	11.52%	-2.91%

CHAPTER 6

CONCLUSIONS

This investigation presents a new penalty force based contact model developed from the sliding joint formulation proposed by Pappalardo et al. (2015) to model the pantograph-catenary interaction. Unlike the sliding joint formulation, the new formulation derived using the elastic contact approach allows for modeling the loss of contact scenario. The proposed contact formulation requires a single gradient vector and therefore it can be used with the gradient deficient as well as the fully parameterized ANCF elements (Hamper et al., 2015; Ren H., 2015; Shabana 2015). The ANCF cable element was used to model the overhead contact line and the messenger wire. The ANCF approach was found to be appropriate to model the geometric nonlinearities in the catenary system. The multibody model of the pantograph and the ANCF catenary model can be modeled in one single framework of multibody dynamics eliminating the need for co-simulation between the finite element and the multibody dynamics codes. The results obtained with this investigation satisfy the regulation mentioned in the standard EN50317 and match with the results obtained with the sliding joint formulation. Incorporation of the detailed rail- vehicle model helps replicating the reality more closely.

A new approach to model the time varying aerodynamic forces was also incorporated into the model. The drag and the lift forces on the individual pantograph components as well as on the contact wire and the messenger wire are computed at each time-step. The effect of the crosswind was that the aerodynamic uplift force assists the uplift force exerted on the pantograph mechanism increasing the mean contact force by about 11.53%, where the mean contact force value increase when the aerodynamic forces are applied on the pantograph components and the catenary is about 11.52%. The effect of application of aerodynamic forces on the contact wire and the messenger wire seems to be negligible for the considered model. The instability in the motion of the catenary depends on several parameters like the worn out geometric profile of the contact wire, the angle of attack of the flow, wind speed etc. This behavior agrees with the behavior observed in the investigation by Pombo et al. (2009) where a similar pantograph model was used.

As future work, the control strategies could be applied to the new contact model to control the standard deviation and the mean contact force values. This could be helpful in determining the physical control parameters, considering the effect of aerodynamic forces simultaneously. The different wind loading situations can be studied beforehand provided the aerodynamic coefficients are known. The effect of wind on both, the pantograph and the catenary, can be studied for attaining optimal contact force for the high- speed train. Extreme operating conditions can be modeled as well to observe the loss of contact phenomenon. Hence this investigation can be useful to predict wear rates better, model realistic contact scenarios between the pan-head and the contact line which can result into better current collection system designs making the systems more damage-proof and saving significant amount of money in the maintenance.

APPENDIX

Nomenclature

$\mathbf{C}$	vector of constraint equations
$\mathbf{C}_{\mathbf{q}_r}$	constraint Jacobian matrix associated with rigid body coordinates
$\mathbf{C}_e$	constraint Jacobian matrix associated with ANCF coordinates
d	penalty formulation damping coefficient
$\mathbf{e}$	vector of element nodal coordinates of ANCF body
$\bar{\mathbf{G}}^p$	matrix relating the angular velocity vector to the pan-head orientation velocities
k	penalty formulation stiffness coefficient
$\mathbf{L}^p$	Jacobian of position vector of contact point associated with pan-head coordinates
$\mathbf{M}$	mass matrix
$\mathbf{n}^w$	normal vector to the wheel surface at the contact point
$\mathbf{n}^r$	normal vector to the rail surface at the contact point
$\mathbf{p}$	vector of system generalized coordinates
$\mathbf{Q}$	vector of system generalized forces
$\mathbf{Q}_{Penalty}$	vector of penalty contact force
$\mathbf{q}$	vector of generalized coordinates
$\mathbf{r}$	position vector of an arbitrary point
$\mathbf{r}^p$	global position vector of contact point P on pan-head
$\mathbf{r}^c$	global position vector of contact point P on catenary
$\mathbf{S}$	element shape function matrix

s	non-generalized coordinate related to catenary wire
$\mathbf{s}^r$	non-generalized coordinates vector or surface parameters of rail
$\mathbf{s}^w$	non-generalized coordinates vector or surface parameters of wheel
t	time
$\mathbf{t}^w$	tangent vector to the wheel surface at contact point
$\mathbf{t}^r$	tangent vector to the rail surface at the contact point
$x \quad y \quad z$	element spatial coordinates
$\boldsymbol{\omega}$	angular velocity vector
$\boldsymbol{\lambda}$	vector of Lagrange multipliers

REFERENCES

1. Ambrósio, J., Pombo, J., Pereira, M., Antunes, P., & Mósca, A., 2012, "A computational procedure for the dynamic analysis of the catenary-pantograph interaction in high-speed trains", *Journal of Theoretical and Applied Mechanics*, *50*(3), pp. 681-699.

2. Ambrósio, J., Pombo, J., Rauter, F., & Pereira, M., 2009, "A memory based communication in the co-simulation of multibody and finite element codes for pantograph-catenary interaction simulation", *Multibody dynamics, Springer Netherlands*, pp. 231-252.

3. Arnold, M., & Simeon, B., 2000, "Pantograph and catenary dynamics: a benchmark problem and its numerical solution", *Applied Numerical Mathematics*, *34*(4), pp. 345-362.

4. Bocciolone, M., Resta, F., Rocchi, D., Tosi, A., & Collina, A., 2006, "Pantograph aerodynamic effects on the pantograph–catenary interaction", *Vehicle System Dynamics*, *44*(sup1), pp. 560-570.

5. Bae, D. S., and Haug, E. J., 1987A, "A Recursive Formulation for Constrained Mechanical System Dynamics: Part I Open loop Systems", Journal of Structural Mechanics, 15(3), pp. 359-382.

6. Bae, D. S., and Haug, E. J., 1987B, "A Recursive Formulation for Constrained Mechanical System Dynamics: Part II Closed Loop Systems", Journal of Structural Mechanics, 15(4), pp. 481-506.

7. Bruni, S., Ambrosio, J., Carnicero, A., Cho, Y. H., Finner, L., Ikeda, M., and Zhang, W., 2015, "The results of the pantograph–catenary interaction benchmark", *Vehicle System Dynamics*, *53*(3), pp. 412-435.

8. Bruni, S., Bucca, G., Collina, A., & Facchinetti, A., 2012, "Numerical and hardware-in-the-loop tools for the design of very high speed pantograph-catenary systems", *Journal of Computational and Nonlinear Dynamics, 7*(4), 041013.

9. Bucca, G., & Collina, A., 2009, "A procedure for the wear prediction of collector strip and contact wire in pantograph–catenary system", *Wear, 266*(1), pp. 46-59.

10. Carnevale, M., Facchinetti, A., Maggiori, L., & Rocchi, D., 2015, "Computational fluid dynamics as a means of assessing the influence of aerodynamic forces on the mean contact force acting on a pantograph", *Proceedings of the Institution of Mechanical Engineers, Part F: Journal of Rail and Rapid Transit*, 0954409715606748.

11. Collina, A., & Bruni, S., 2002, "Numerical simulation of pantograph-overhead equipment interaction", *Vehicle System Dynamics*, *38*(4), pp. 261-291.

12. de Jalón, J. G., 2007, "Twenty-five years of natural coordinates", *Multibody System Dynamics, 18*(1), pp. 15-33.

13. Facchinetti, A., & Bruni, S., 2012, "Hardware-in-the-loop hybrid simulation of pantograph–catenary interaction", *Journal of Sound and Vibration, 331*(12), pp. 2783-2797.

14. Facchinetti, A., Gasparetto, L., & Bruni, S., 2013, "Real-time catenary models for the hardware-in-the-loop simulation of the pantograph–catenary interaction", *Vehicle System Dynamics*, *51*(4), pp. 499-516.

15. Gere, J. M., & Weaver, W., 1965, *Analysis of framed structures*, Van Nostrand, New York.

16. Gerstmayr, J., & Shabana, A. A., 2006, "Analysis of thin beams and cables using the absolute nodal co-ordinate formulation", *Nonlinear Dynamics*, *45*(1-2), pp. 109-130.

17. Hamper, M. B., Wei, C., and Shabana, A. A., 2015, “Use of ANCF Surface Geometry in the Rigid Body Contact Problems: Application to Railroad Vehicle Dynamics”, *Journal of Computational and Nonlinear Dynamics, 10*(2), pp. 1-12.

18. Ikeda, M., & Mitsumoji, T., 2009, “Numerical estimation of aerodynamic interference between panhead and articulated frame”, *Quarterly Report of RTRI*, *50*(4), pp. 227-232.

19. Lankarani, H. M., & Nikravesh, P. E., 1994, “Continuous contact force models for impact analysis in multibody systems”, *Nonlinear Dynamics*, *5*(2), pp. 193-207.

20. Lee J.H. and Park T. W., 2012,” Development of a three-dimensional catenary model using the cable elements based on absolute nodal coordinate formulation”, *Journal of Mechanical Science and Technology,* 26(12), pp. 3933-3941.

21. Massat, J. P., Laine, J. P., & Bobillot, A., 2006, “Pantograph–catenary dynamics simulation”, *Vehicle System Dynamics*, *44*(sup1), pp. 551-559.

22. Pappalardo, C. M., 2015, “A natural absolute coordinate formulation for the kinematic and dynamic analysis of rigid multibody systems”, *Nonlinear Dynamics*, *81*(4), pp. 1841-1869.

23. Pappalardo, C. M., Patel, M. D., Tinsley, B., & Shabana, A. A., 2015, “Contact force control in multibody pantograph/catenary systems”, *Proceedings of the Institution of Mechanical Engineers, Part K: Journal of Multi-body Dynamics*, 1464419315604756.

24. Poetsch, G., Evans, J., Meisinger, R., Kortüm, W., Baldauf, W., Veitl, A., and Wallaschek, J., 1997, “Pantograph/catenary dynamics and control”, *Vehicle System Dynamics*, *28*(2-3), pp. 159-195.

25. Pombo, J., & Ambrósio, J., 2012, "Influence of pantograph suspension characteristics on the contact quality with the catenary for high speed trains", *Computers & Structures*, *110*, pp. 32-42.

26. Pombo, J., Ambrósio, J., Pereira, M., Rauter, F., Collina, A., and Facchinetti, A., 2009, "Influence of the aerodynamic forces on the pantograph–catenary system for high-speed trains", *Vehicle System Dynamics*, *47*(11), pp. 1327-1347.

27. Ren, H., 2015, "A Simple Absolute Nodal Coordinate Formulation for Thin Beams with Large Deformations and Large Rotations", *Journal of Computational and Nonlinear Dynamics*, *10*(6), 061005.

28. Seo, J. H., Kim, S. W., Jung, I. H., Park, T. W., Mok, J. Y., Kim, Y. G., and Chai, J. B., 2006, "Dynamic analysis of a pantograph–catenary system using absolute nodal coordinates", *Vehicle System Dynamics*, *44*(8), pp. 615-630.

29. Seo, J. H., Sugiyama, H., & Shabana, A. A., 2005, "Three-dimensional large deformation analysis of the multibody pantograph/catenary systems", *Nonlinear Dynamics*, *42*(2), pp. 199-215.

30. Shabana, A. A., 1998, "Computer implementation of the absolute nodal coordinate formulation for flexible multibody dynamics", *Nonlinear Dynamics*, *16*(3), pp. 293-306.

31. Shabana A.A., 2010, *Computational Dynamics, Third Edition, Wiley, Hoboken, New Jersey*.

32. Shabana, A. A., *Dynamics of multibody systems, 4th Edition 2013, Cambridge university press*.

33. Shabana, A. A., 2015, “Definition of ANCF Finite Elements”, *Journal of Computational and Nonlinear Dynamics*, *10*(5), pp. 1-5.

34. Shabana, A. A., & Yakoub, R. Y., 2001, “Three dimensional absolute nodal coordinate formulation for beam elements: theory”, *Journal of Mechanical Design*, *123*(4), pp. 606-613.

35. Stickland, M. T., & Scanlon, T. J., 2001, “An investigation into the aerodynamic characteristics of catenary contact wires in a cross-wind”, *Proceedings of the Institution of Mechanical Engineers, Part F: Journal of Rail and Rapid Transit*, *215*(4), pp. 311-318.

36. Stickland, M. T., Scanlon, T. J., Craighead, I. A., & Fernandez, J., 2003, “An investigation into the mechanical damping characteristics of catenary contact wires and their effect on aerodynamic galloping instability”, *Proceedings of the Institution of Mechanical Engineers, Part F: Journal of Rail and Rapid Transit*, *217*(2), pp. 63-71.

37. Yakoub, R. Y., & Shabana, A. A., 2001, “Three dimensional absolute nodal coordinate formulation for beam elements: implementation and applications”, *Journal of Mechanical Design*, *123*(4), pp. 614-621.

VITA

Name	Shubhankar Kulkarni
Education	**University of Illinois at Chicago, USA** M.S. / Mechanical and Industrial Engineering (2013- Present)
	University of Pune, India B.E. / Mechanical Engineering (2008-2012)